A Seismic Channel Model: The San Ramon Fault

Hector Torres-Silva[1], Diego Torres Cabezas[2]

[1] Escuela Universitaria de Ingeniería Eléctrica-Electrónica. Universidad de Tarapacá. Avda. 18 de Septiembre 2222, Casilla Postal 6-D. Arica, Chile.
[2] Departamento Tecnologías de Información. Dirección del Trabajo, Agustinas 1253, Of. 509. Santiago, Chile.

Abstract— *Although seismic waves have been studied for many years, their soliton structure has only recently studied. Deformation solitons propagate along earthquake faults and can induce large earthquakes. Rotation solitons are generated in earthquake sources and propagate throughout the Earth. The conclusion to be reached from our paper is that the research on seismic solitons is essential for investigating the propagation of seismic waves and helps understand mechanisms triggering earthquakes. This paper discusses the development of elastodynamics equations similar to Maxwell's equations in a chiral -mode which is applied to a seismic channel, which is dispersive and nonlinear. The chirality is described in terms of the formalism proposed by Born-Fedorov. The nonlinearity is Kerr-type, and dispersion of the medium is taken into account explicitly through the Taylor series expansion. Through numerical calculations these theoretical results allow us analyze the soliton propagation of S-seismic pulses which can induce strong earthquakes. The numerical calculation is applied to the San Ramon Fault localized in Santiago City, Chile which is a seismically active fault that is a main element to be considered in any study on seismic hazard assessment for this city.*

I. INTRODUCTION

Paleoseismic studies of a prominent fault scarp at the west flank of the Andes in Santiago, Chile (The San Ramón Fault) were published recently. The San Ramón Fault (SRF) has been recently identified like a geologically active fault which can produce large magnitude crustal earthquakes, in the range of $M_W \square 6.9 – 7.4$ [1-6]. Figure 1 shows the geomorphologic map of the San Ramón fault. Seismic moment can be estimated with a fixed rupture width of 30 km, consistent with the structure of the SRF at depth (Armijo et al., 2010; Pérez et al., 2013) and 5 m of average slip. In that case, assuming that the fault scarp is either 15 km long, according to the most emergent part of the scarp, or 35 km long if considering the entire well-recognized SRF (Armijo et al., 2010), predicts $M_W \square 7.25$ and $M_W \square 7.5$, respectively. Those magnitude estimates would imply surface rupture and significantly stronger ground motion (and destructive effects) for Santiago (Pérez et al., 2013; Pilz et al., 2011).

Using 5 m
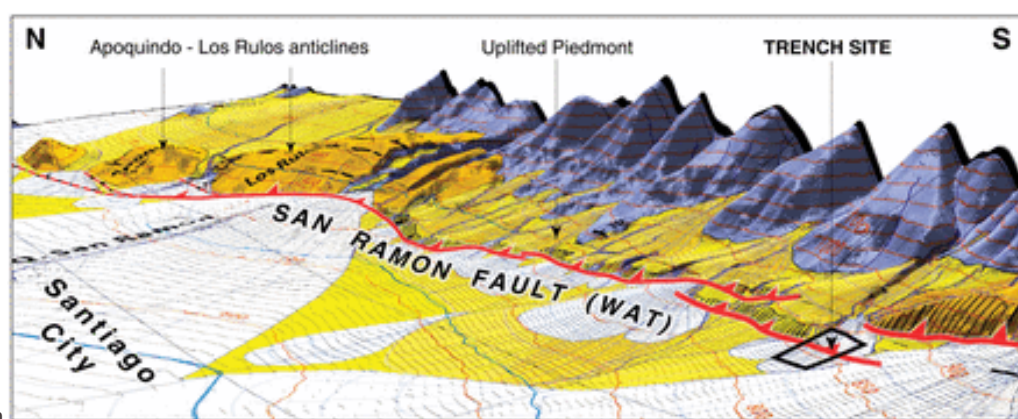
Fig.1: The San Ramón fault scarp, Chile (WAT—west Andean thrust). The geomorphologic map (Armijo et al., 2010) is draped over a 9 m digital elevation model. The San Ramón fault forms a continuous scarp that limits to the west the uplifted piedmont covered with Quaternary alluvium and incised by streams (early-middle Pleistocene in yellow tones, late Pleistocene–Holocene in white).

To further investigate site conditions in the Santiago basin we must consider different locations of possible hypocentres along the San Ramón Fault, a multikilometric frontal thrust at the western front of the Main Cordillera, which has been shown to pose a significant seismic hazard for the city (Armijo *et al.* 2010). The best surface expression of the San Ramón Fault is found along an around 15 km long segment with a sharp fault trace in the 25 km long part separating the rivers Mapocho and Maipo along the San Ramón mountain front (see Fig. 1).

In this paper we propose a model to estimate the magnitude of earthquakes along the fault of the SRF which acts as a seismic channel which develops a soliton pulse acting as earthquake source. Rotational motions in earthquake sources naturally generate rotational seismic waves [7-10].

The difference in speed of travel of P-waves and S-wave is vital to transmit energy of seismic wave. The P wave is a *longitudinal* wave or a *compression* wave. Force is applied in the direction that the wave is travelling. In S wave, the medium is displaced in a *transverse* (up and down - compared to the line of travel) way, and the medium must *shear* or "move away" from the material right next to it to cause the shear and transmit the wave. This take more time, and this is why the S wave moves more slowly than the P wave in seismic events. Here we model the SRF like a seismic channel using a chiral approach [11-13].

There are two types of tectonic solitons which can be excited in the earthquake source and propagating along the fault: longitudinal self-distortion (plastic) solitons and shear self-distortion solitons. The Earth's interior is modeled as an elasto-plastic continuum and elastoplastic waves [9, 10], that describe elastic longitudinal and plastic shear distortion solitons. We apply similar method in order to determine the solitons propagating along the fault SRF. The type of soliton studied here is seismic shear self-distortion Schrödinger's solitons which may propagate slowly along the fault and trigger new strong earthquakes. Our main results (equation 20) is obtained under the chiral approach [11-13].

The chirality was first observed as optical activity and corresponds to the rotation of the plane of polarization in linear isotropic materials. The Born-Fedorov equations for electromagnetic system are given by [14, 15].

$$D = \varepsilon \left(\vec{E} + T_c \nabla \times \vec{E} \right) \qquad (1)$$

$$B = \mu \left(\vec{H} + T_c \nabla \times \vec{H} \right) \qquad (2)$$

The pseudoscalar T_c represents the measure of chirality and has units of length. The validity of equations (1) and (2) has been demonstrated in studies of chiral electrodynamics [11] and from an electromagnetic point of view, chiral soliton

pulse can be described by specific equations [12]-[13]. By analogy between elastodynamics and electrodynamics in this work we use these Born-Fedorov equations which are the most suitable to study SRF like a seismic channel. Here the electric permittivity is equivalent density of matter $\varepsilon \to \rho$, the magnetic permeability is equivalent to the inverse of the Lamé parameter $\mu \to 1/\mu_s$. The speed of transversal seismic S- waves is given by $\sqrt{\rho/\mu_s}$ [14, 15] and changes of the polarization of transverse seismic waves are take into account during their propagation through the SRF.

II. BASIC EQUATION FOR ROTATIONAL PROPAGATION.

Using equations (1) and (2), we obtain in the analogous framework under this section the nonlinear Schrödinger equation for a chiral seismic channel. (S-type waves)

$$D_S = \rho_n \vec{E}_S + \rho T_c \left(\nabla \times \vec{E}_S \right) \qquad (3)$$

$$B_S = 1/\mu_s (\vec{H}_S + T_c \left(\nabla \times \vec{H}_S \right)) \qquad (4)$$

These equations are symmetric under duality transformations and temporal reversibility, ρ_n is the density of matter and T_c the chiral rotational seismic coefficient. The corresponding like Maxwell equations are

$$\nabla \times \vec{H}_S = \frac{\partial \left(\rho_n \vec{E}_S \right)}{\partial t} + \sigma \vec{E}_S + \frac{\partial}{\partial t} T_c \left(\nabla \times \vec{E}_S \right) = \frac{\rho_n \partial \vec{E}_S}{\partial t} + \sigma \vec{E}_S + \rho T_c \nabla \times \frac{\partial \vec{E}_S}{\partial t}$$
$$(5)$$

$$\nabla \times \vec{E}_S = -\frac{\partial \vec{B}_S}{\partial t} = -(1/\mu_s)\frac{\partial \vec{H}_S}{\partial t} - (1/\mu_s)T_c \frac{\partial \left(\nabla \times \vec{H}_S \right)}{\partial t} \quad (6)$$

Taking the rotational of the equation (6) and considering the following approximations

$$\nabla \cdot D_S \, \Box \, 0 = \rho_n \nabla \cdot \vec{E}_S + \rho T_c \nabla \cdot \nabla \times \vec{E}_S \; ; \; \nabla \cdot \vec{E}_S \cong 0 \to \nabla \rho_n \to 0$$

$$\nabla \cdot B_S = 0 \Rightarrow \nabla \cdot \vec{H}_S = 0$$

We obtain the following wave equation

$$\nabla^2 \vec{E}_S + (1/\mu_s)\rho T_c^2 \frac{\partial^2}{\partial t^2} \nabla^2 \vec{E}_S = (1/\mu_s)\rho_n \frac{\partial^2 \vec{E}_S}{\partial t^2}$$
$$+(1/\mu_s)\sigma \frac{\partial \vec{E}_S}{\partial t} + \left((1/\mu_s)\rho_n T_c + (1/\mu_s)\rho \right) T_c \nabla \times \frac{\partial^2 \vec{E}_S}{\partial t^2} \quad (7)$$
$$+(1/\mu_s)\sigma T_c \nabla \times \frac{\partial \vec{E}_S}{\partial t}$$

Here we assume that the chiral seismic medium is of a Kerr nonlinearity type, described by a refractive index such that the seismic permittivity is

$$\rho_n = \rho_S + \rho_2 \left| \vec{E}_S \right|^2 \qquad (8)$$

where ρ_s is the linear part and ρ_2 is the nonlinear component respectively of ρ_n σ is the rock conductivity loss. Past studies have demonstrated that the slip type or style of faulting is potentially significant for correlating earthquake magnitude and rupture parameters. To categorize the dominant slip type for SRF in this paper, we use a simple scheme based on equation (8).

From equation (8) we can be inferred easily the expression for the index of refraction as in [8]. Replacing ρ_n into equation (7) we obtain

$$\nabla^2 \vec{E}_s + (1/\mu_s)\rho_s T_c^2 \frac{\partial^2 \vec{E}_s}{\partial t^2}\nabla^2 \vec{E}_s = (1/\mu_s)\rho_s \frac{\partial^2 \vec{E}_s}{\partial t^2}$$
$$+(1/\mu_s)\sigma\frac{\partial \vec{E}_s}{\partial t} + (1/\mu_s)\rho_2\left|\vec{E}_s\right|^2\frac{\partial^2 \vec{E}_s}{\partial t^2} +$$
$$2(1/\mu_s)\rho_s T_c \nabla\times\frac{\partial^2 \vec{E}_s}{\partial t^2} + (1/\mu_s)T_c\rho_2\left|\vec{E}_s\right|^2\nabla\times\frac{\partial^2 \vec{E}_s}{\partial t^2}$$
$$+(1/\mu_s)T_c\sigma\nabla\times\frac{\partial \vec{E}_s}{\partial t} \tag{9}$$

Assuming that $\vec{E}_s$ represents a localized waveform, which propagates in the z direction, it has

$$\vec{E}_s\left(\vec{r},t\right) = \left(\hat{x}+j\hat{y}\right)\Psi\left(\vec{r},t\right)e^{-j(kz-\omega_0 t)} = \vec{\Psi}e^{-j(kz-\omega_0 t)} \tag{10}$$

where $\vec{\Psi}$ represents the complex envelope. To solve the equation (9) the property of the Fourier transform $\partial^2/\partial t^2 \leftrightarrow -\omega_0^2$ is applied, and then we determine the operators ∇^2 and $\nabla\times$.

After several algebraic manipulations the result is as follows

$$\left(1-T_c^2 k_0^2\right)\left(-2jk_0\frac{\partial\vec{\Psi}}{\partial z}-k_0^2\vec{\Psi}\right)$$
$$-\frac{1}{v^2}\left(2j\omega_0\frac{\partial\vec{\Psi}}{\partial t}-\omega_0^2\vec{\Psi}\right)= \tag{11}$$
$$2\zeta k_0^3\vec{\Psi} + j\omega_0\alpha\left(1-T_c k_0\right)\vec{\Psi}$$
$$-\beta\omega_0^2\left|\vec{\Psi}\right|^2\left(1-T_c k_0\right)\vec{\Psi}$$

where $\quad v_s^2 = \mu_s\frac{1}{\rho_s}\ ;\qquad \alpha = (1/\mu_s)\sigma\ ;\qquad k_0 v = \omega_0\ ;$

$\beta = (1/\mu_s)\rho_2,\quad j = \sqrt{-1}$. To get to the equation (13) the approximation of small amplitudes is also considered, given by

$$\left|\frac{\partial^2\vec{\Psi}}{\partial z^2}\right| \Box\ \left|j2k\frac{\partial\vec{\Psi}}{\partial z}\right|, \left|\frac{\partial\vec{\Psi}}{\partial t}\right|\Box\ \left|j\omega_0\vec{\Psi}\right|, \left|\frac{\partial^2\left|\vec{\Psi}\right|^2\vec{\Psi}}{\partial t^2}\right|\Box\ \left|j\omega_0\frac{\partial\left|\vec{\Psi}\right|^2\vec{\Psi}}{\partial t}\right|\Box\ \left|j\omega_0\left|\vec{\Psi}\right|^2\vec{\Psi}\right|$$

To illustrate the difference between the high frequency and the low frequency in an earthquake we show the figure 2, which corresponds to the strong earthquake February 27, 2010, Chile. Here we have a set of measurements of high-frequency energy radiation. The upper, middle and lower traces are an observed seismogram, the squares of the band-pass (2-4 Hz) filtered seismogram, and its smoothed time series (normalized by the maximum value), respectively. "A" and "F" in the lower trace denote the arrival of P-wave and estimated end of high frequency energy radiation, respectively (ω_0 have correspondence with the upper signal of high frequency> 10 radians/seg and $\frac{\partial}{\partial t}$ have correspondence with the lower signal of slow frequency) [14, 18]. In our analysis we assume that a possible earthquake in San Ramon Fault waveforms can be similar but of lower amplitude to those shown in Figure 2
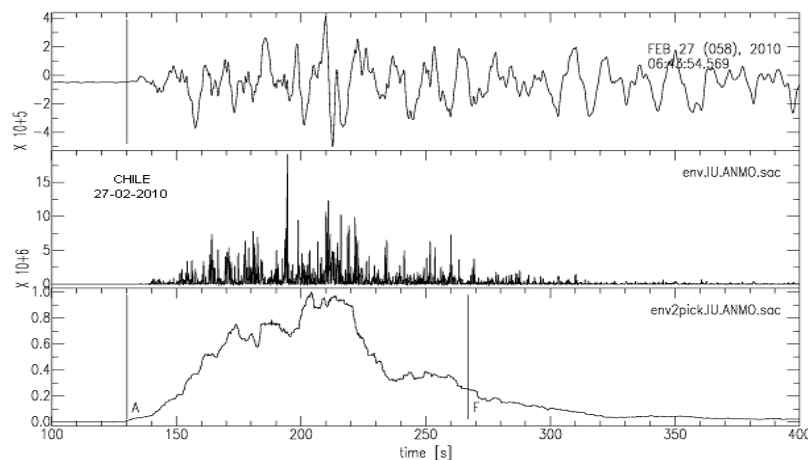
Fig.2: A measurement of high frequency energy radiation of the February 27, 2010 Chile Earthquake, the bottom graph shows the low frequency signal which is the envelope of the high frequency wave. In the next section this envelope is modeled as a Gaussian pulse.

The effect of dispersion is included heuristically. Making the change of variables $\phi = 2k_0\vec{\Psi}$ y $z^* = \frac{z}{1-T_c^2k_0^2}$ and rearranging the terms of equation (11) we obtain

$$j\left[\frac{\partial\phi}{\partial z^*} + \frac{1}{v}\frac{\partial\phi}{\partial t}\right] = -(1-k_0T_c)\frac{j\omega\alpha}{2k}\phi$$

$$-\frac{\beta\omega_0^2}{(2k)^3}(1-k_0T_c)|\phi|^2\phi \qquad (12)$$

$$+k_0^2T_c\left(1-\frac{k_0T_c}{2}\right)\phi$$

As the envelope $\Psi(z,t)$ is a slowly varying function of in z and t, the dispersion relation $k = k(\omega)$ can be transformed to the domain of spatial variations by means of $\Delta\omega = \omega - \omega_0$, which is a small deviation of the sideband frequency with respect to ω_0, and through $\Delta k = k - k_0$, which represent the corresponding wave number.

Using the Fourier transform for Δk, $\Delta\omega$, approximating $\frac{1}{v} \square \frac{\Delta k}{\Delta\omega}$, and using the Taylor series we obtain

$$\Delta k = \frac{1}{v}\frac{\partial}{\partial t} = \frac{\partial k}{\partial\omega}\frac{\partial}{\partial t} - j\frac{1}{2}\frac{\partial^2 k}{\partial\omega_0^2}\frac{\partial^2}{\partial t^2} + ... = \frac{k_0}{\omega_0}\frac{\partial}{\partial t}$$

By substituting this operator in equation (14), we obtain

$$j\frac{\partial\phi}{\partial z^*} + \frac{1}{v_g}\frac{\partial\phi}{\partial t} + \frac{1}{2}k''\frac{\partial^2\phi}{\partial t^2} + (1-k_0T_c)\frac{j\omega\alpha}{2k_0}\phi - (1-k_0T_c)\frac{\beta\omega_0^2}{(2k)^3}|\phi|^2\phi$$

$$+\left(1-\frac{k_0T_c}{2}\right)T_c k_0^2\phi = 0$$

$$(13)$$

where

$$k' = \frac{\partial k}{\partial\omega} = \frac{1}{v_g}; \ k'' = \frac{\partial^2 k}{\partial\omega^2};$$

Equation (13) describes the propagation of pulses in a chiral, rotational, dispersive and non linear channel [13].

The first term represents the evolution of the pulse with distance. The second, and third terms represents the scattering of a seismic chiral channel $k'\left(=\frac{1}{v_g}\right)$ and k'' corresponds to the chromatic dispersion k', indicating that the pulse moves with the group velocity, while the dispersion of the group velocity (GVD) is represented by k'', which alters the relative phases of the frequency components of pulse widening, producing its temporal expansion. The fourth is associated with attenuation (α), in this case such losses are weighted by the seismic chirality. The fifth term $|\phi|^2\phi$ represents nonlinear effect, like a Kerr effect, which is

characterized by having a refractive index dependent on the seismic field intensity and related to the slip type that can alter and widen the spectrum of frequency. This term also depends on the chiral factor. Finally, the last term is clearly associated with the chirality of the seismic channel.

III.   ANALYSIS AND SIMULATIONS

In order to ease up the solution of the propagation equation the following change of variables is introduced: $t^* = t - \frac{Z}{v_g}$,

$z^* = Z$

Defining

$$v_S^2 = \mu_S\frac{1}{\rho_S}; \ \alpha = (1/\mu_S)\sigma; \ k_0 = \frac{\omega_0}{v}; \ \beta = (1/\mu_S)\rho_2$$

$$C = 1 - k_0T_c \quad (14)$$

$$q = 2k_0\phi, \ Z = \frac{z}{1-\zeta^2k_0^2}, k_0 = \frac{\omega_0}{v}, \ v_g = \frac{1}{k'} = \frac{1}{\partial k/\partial\omega},$$

$$k'' = \frac{\partial^2 k}{\partial\omega^2}, \qquad (15)$$

We have

$$j\frac{\partial q}{\partial Z} = -\frac{1}{2}k''\frac{\partial^2 q}{\partial t^{*2}} - j\frac{\omega_0\alpha C}{2k_0}q + \frac{\beta\omega_0^2\alpha}{(2k_0)^3}|q|^2 q$$

$$(16)$$

Finally, is useful normalize the Eq. (16) by introducing

$$\tau = \frac{t^*}{t_0} \qquad (17)$$

Let us model heuristically the relationship between the wave amplitude and the initial seismic power as follows

The normalized amplitude q (equation 16) is proportional to

$$\sqrt{\frac{P_S}{P_{ref}}} \ \text{or} \ \sqrt{\frac{P_S t_S}{P_{ref} t_{ref}}} = \sqrt{\frac{E_S}{E_{ref}}}$$

Where P_S is the power earthquake, P_{ref} is the power reference and t_S is the time duration of the earthquake, $t_S = t_{ref}$, so using the empirical equation of Gutemberg and Richer [16] which is useful for magnitude of shallow, small-moderate nearby earthquakes

$$\log E_S = 11.8 + 1.5M$$

$$(18)$$

We have

$$\frac{E_S}{E_{ref}} = e^{\sqrt{0.12(M_S - M_{ref})}}$$

We use this empirical equation because this theory gives a relationship between the magnitude M_S and the energy released E_S which only tends to saturate for really great earthquakes.

Thus we can model the S-wave q through the transformation

$$q(Z,\tau) = e^{\sqrt{0.12(M_S - M_{ref})}} e^{-\frac{\alpha \omega_0 C}{2k_0} Z} U(Z,\tau)$$
(19)

where M_S is the peak magnitude of the soliton and M_{ref} is the reference magnitude for a weak seism which acts as calibration standard. Finally the expression (16) can be scaled as

$$j\frac{\partial U}{\partial Z} = -\frac{1}{2}\frac{k''}{t_0^2}\frac{\partial^2 U}{\partial \tau^2} + \frac{\beta \omega_0^2}{(2k_0)^3} e^{\sqrt{0.12(M_S - M_{ref})}} e^{-\frac{\alpha \omega_0}{k_0} CZ} |U|^2 U$$
(20)

To our knowledge this is the first time that the magnitude M_S of earthquake is considered into the nonlinear Schrodinger equation. Through numerical calculations these theoretical results (eqs 14-20), would allow analyze the effects of chirality on the attenuation of equation (20) for propagation of S-seismic pulses. Also we take into account the magnitude M_S of moderate earthquakes along the SRF which can trigger strong earthquakes in Santiago City.

To solve the pulse propagation in nonlinear dispersive media we use the split-step Fourier method. The relative speed of this method compared with most FD methods can be attributed in part to the use of finite-Fourier-transform (FFT) algorithm [17]. In general, linear and nonlinear parts of equation (19) act together along the length of the earthquake. The split-step method obtains an approximate solution by assuming that in propagation the seismic field over a small distance Δz, is carried out in two steps. In the first step, from $Z = Z_0$ to $Z = Z_0 + \Delta Z/2$, the linear part acts alone, and the non linear part is zero. In the second step, the nonlinearity acts alone in the point $\Delta Z/2$, (linear part is null).

For the simulation we consider an average of velocity v_S because the bedrock of SRF is layered with $v_S = 2.500 m/s$ between 0 and 2.2 km depth, $v_S = 3.300 m/s$ between 2.2 km and 8 km depth (Barrientos et al. 2004) [19]. The frequency w_0 was set to $> 10 radians/s$ in this simulation. The wave comes to 8 km deep in the bedrock.

Figure 3. shows the Intensity U calculated numerically from equation (20). The parameters correspond to a weak earthquake with $M_S = 1$, M_{ref} is the reference magnitude for a

weak seism which acts as calibration standard to nonlinear Schrodinger equation with $M_s > 1$. Here $T_c = 0$, $C = 1$ the chiral effect is not considered. The angle θ between the plane which contains U and axis Z, $\theta = 0$. The normalized attenuation $\frac{\alpha \omega_0}{k_0}$ is neglected for short distance, $Z \square 30 km$.
The equation (20) is reduced to

$$j\frac{\partial U}{\partial Z} = -\frac{1}{2}\frac{k''}{t_0^2}\frac{\partial^2 U}{\partial \tau^2} + \frac{\beta \omega_0^2}{(2k_0)^3} |U|^2 U$$

Which is the typical result obtained by other authors [7, 9].
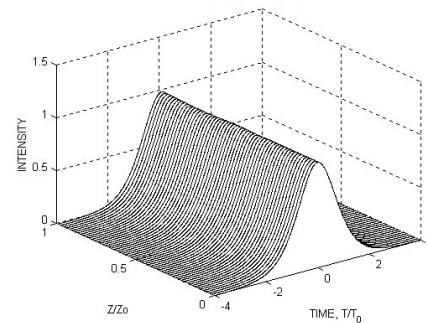
Fig.3: Parameters of a weak earthquake; $M_{ref} = 1$, $M_S = 1$,

$$k_0 v_S = W_0, T_c = 0, C = 1$$

$\sqrt{\rho/\mu_S} = 3 km/s$ $\rho_S = 4 g/cm^\wedge 3$ $\rho_2 = 10^{-4}$ $Z_0 = 30 km$,

$\beta = (1/\mu_S)\rho_{2 = 10^{-3}}$, $C = 1$, $\theta = 0$, depth = 8km

The propagating shear wave is represented by a Gaussian pulse simulating the bottom graph of figure 2

Figure.4. shows the envelope of U for a strong earthquake with $C = 1 - k_0 T_c = 0.3$, nearly of $Z = 30 km$ we have a peak of U, which it indicates that the maximum of U can trigger a major earthquake. From equation (20) we can obtain $M_S - M_{ref} \approx 6.4$, that is $M_S \approx 7.4$. This value agrees with the estimations of Vargas, Armijo y Pérez [1, 2, 3] respectively who are used the Wells – Coppersmith's semi empirical approach [6]. We note that in this paper $M_W \square M_S$ because M_S only tends to saturate for really great earthquakes $M_W > 8.0$. The properties of rock in the seismic wave travel path are important because they directly influence the amplitudes of seismic waves. Rock is normally considered to be stable with respect to seismic amplification, but here we show that this is not always the case. The wavelength of a seismic wave of a given frequency is proportional to its velocity. $v_g = v_S = \lambda f$. If a shear wave passes into a lower velocity medium, it will reduce its wavelength so to conserve

energy, the wave is amplified. Sedimentary basins have lower velocities than bedrock and can therefore produce intense amplification of incoming seismic waves. As seismic wave travel faster through harder denser rocks and compact sediments than through soft rocks and loose sediments.The change in velocity also changes the rate at which seismic energy is amplified. As a wave travels up to the layer with sediment (nearly of $Z = 30km$), density decreases (as does the impedance), therefore the shear wave velocity also decreases. If Energy is to remain constant when wave approaches the surface, the particles velocity must increase to compensate the decrease in density and shear wave velocity producing a large effect on the basin layer. Sediment impedance affects the amplitude of earthquake ground motion. When $Z > 30km$, the S-wave along the rock layer decreases due to the drastic change of impedance between the rock and the sediment layer. Impedance is the product of the density (ρ_S), the shear wave velocity (v_S) and the cosine of the angle of incidence which is defined as the angle between the vertical and the direction of seismic wave propagation. In terms of angle θ_S the change in impedance is expressed with the impedance contrast $I_C = \rho_S V_S \sin \theta_S / \rho_b V_b$

. At $Z_0 = 30km$ the reflection coefficient is $r_C = \rho_S V_S \sin \theta_S - \rho_b V_b /(\rho_S V_S \sin \theta_S + \rho_b V_b)$ with

$I_C = \rho_S V_S \sin \theta_S / \rho_b V_b >> 1$ the S-wave has a peak with $M_S > 7$, that is the energy E reaches a maximum that is transferred to the basin layer where seismic waves are trapped and begin to reverberate.

Thus we can see that the chiral factor C contributes to the S wave to be amplified. Consequently the S wave travels further along the fault.
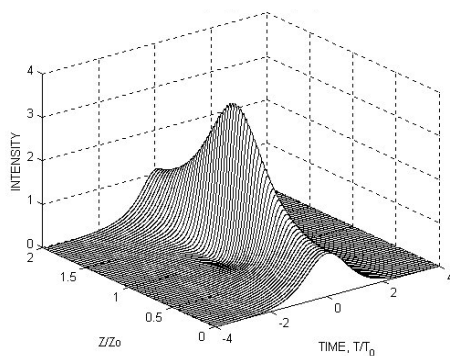
Fig.4: Parameters of a strong earthquake, Peak of $M_S > 7$,

$$M_{ref} = 1, \ C = 1 - k_0 T_C = 0.3$$

$\sqrt{\rho / \mu_S} = 3km/s$, $\rho_S = 4g/cm^3$, $\rho_2 = 10(-4)$ $Z_0 = 30km$, $w > 10$ radians/s. $\theta = 15°$, depth = 8km

As we can see, rotational tectonic waves can propagate along the fractured tectonic fault like SFR with a speed of 2-4 km per second. These waves may have a form of rotational seismic solitons and can trigger major earthquakes. Thus, the research on rotational seismic solitons is essential for investigating the propagation of seismic waves and helps understand mechanisms triggering earthquakes. Chiral rotational seismic waves propagate faster in solid rocks and much slower in fractured media along tectonic faults. A rupture breaking the free surface is another important element to keep in mind in order to improve future kinematic rupture scenarios for the SRF region. Indeed. In this model further improvements should include local site/soil effects and basin/topographic effects.

IV.   CONCLUSIONS

In this paper we have obtained the Schrödinger nonlinear equation for a channel whose core is chiral, dispersive and has nonlinear behavior. The effect of chirality is manifested by the terms associated with the loss of the chiral channel and the nonlinear coefficient. The most significant result of our work is that to use the chirality of S waves can cancel out the losses and nonlinearities of the channel, which would allow us to modify radically their behavior as channel of seismic soliton. Numerical calculation of the equation was obtained, to model by soliton in the SRF. We propose that the San Ramón Fault is not only a geologically active fault, but also it presents seismicity that can be associated with this structure at and resulting in a seismically active fault too. As seismic waves travel though the ground, they travel faster through hard rock than soft soil. As a result, when the waves move from hard rock to soft soil, the amplitude (largeness) of the waves needs to increase to be able to carry the same amount of energy, creating stronger shaking. This same principle accounts for the site effects of sediment thickness. The deeper the sediment above bedrock, the more soft soil there is for seismic waves to travel through, therefore creating stronger amplifications. This is a main element to be considered in any study on seismic hazard assessment for the city of Santiago, Chile. Through numerical calculations our theoretical results would allow analyze the propagation of S-seismic pulses that can trigger strong earthquakes in this city.

REFERENCES

[1] Vargas G et al, 2014, Probing large intraplate earthquakes at the west flank of the Andes, Geology,

published on line on 17 October 2014 as doi: 1130/35741.1.

[2] Armijo R., et al ,2010, The West Andean thrust, the San Ramón fault and the seismic hazard for Santiago, Chile: Tectonics, v. **29**, TC2007.

[3] Pérez A et al, 2013,Improving seismotectonics and seismic hazard assessment along the san Ramón fault at the eastern border of Santiago city, Chile: Natural Hazards, v. **71**, p.243–274.

[4] Brooks B.A., et al, 2011, Orogenic-wedge deformation and potential for great earthquakes in the central Andean backarc: Nature Geoscience, v. **4**, p. 380–383.

[5] Pilz M et al 2011, Modelling basin effects on earthquake ground motion in the Santiago de Chile basin by a spectral element code: Geophysical Journal International, v. **187**, p. 929–945.

[6] Wells D and Coppersmith K, (1994) New Empirical Relationships among Magnitude, Rupture Length, Rupture Width, Rupture Area, and Surface Displacement, Bulletin of the Seismological Society of America, Vol. 84, No. 4, pp. 974-1002,

[7] Teisseyre K P, (2007), Analysis of a group of seismic events using rotational components*,* Acta Geophys. 55, 535–553.

[8] Teisseyre, R. (2009). New developments in the physics of rotational motions, Bull. Seismol. Soc. Am. 99, no. 2B, 1028–1039.

[9] Erofeyev VI (2003) Wave processes in solids with microstructure. World Scientific, Singapore

[10] Teisseyre R, Yamashita T (1999) Splitting stress motion equations into seismic wave and fault-related fields. Acta Geophys Pol **47**: 2, 135-147

[11] Lakhtakia A, et al 1985. "Time-Harmonic Electromagnetic Fields in Chiral Media" Lecture Notes in Physics 335, Springer-Verlag.

[12] Torres Silva H, 2003, Effect of Chirality on Soliton in Optical Fiber, The Journal Mathematics and Computers in Simulation, vol 62, pp 149-161.

[13] Torres-Silva H, 2004, Non-linear polarization and chiral effects in birefringent solitons, Pramana Journal of Physics Vol. 62 Nº 1 Pág. 37.

[14] Torres-Silva H and Lopez-Bonilla J L(2011). Early Prediction and detection of Strong Earthquakes through Chiral Radiation Waves*,* Journal of Vectorial Relativity, 6, 2, 1-11.

[15] Torres-Silva H, Torres Cabezas D (2013), Chiral Seismic Attenuation with Acoustic Metamaterials, Journal of Electromagnetic Analysis and Applications**,**Vol.5 No.1,

[16] Gutemberg B and Richer C F, (1956), Ann. Geoph.9, 1.

[17] Agrawal G, Nonlinear Fiber Optics, Academic Press, Inc., 1995.

[18] Torres-Silva H et al, (2015), Chiral ratio of the compressional and shear velocity for the determination of strong earthquake, Journal of Science, Engineering and Technology, Vol. 11, No. I, pp 20-28.

[19] Barrientos, S et al (2004): Crustal seismicity in central Chile, Journal of South American Earth Sciences 16, 759-768.